

## Extending in Situ Attenuated-Total-Reflection Surface-Enhanced Infrared Absorption Spectroscopy to Ni Electrodes

Sheng-Juan Huo,<sup>†</sup> Xiao-Kang Xue,<sup>†</sup> Yan-Gang Yan,<sup>†</sup> Qiao-Xia Li,<sup>†</sup> Min Ma,<sup>†</sup> Wen-Bin Cai,<sup>\*,†,‡</sup> Qun-Jie Xu,<sup>‡</sup> and Masatoshi Osawa<sup>§</sup>

Shanghai Key Laboratory for Molecular Catalysis and Innovative Materials and Department of Chemistry, Fudan University, Shanghai 200433, China, Department of Environmental Engineering, Shanghai University of Electric Power, Shanghai 200090, China, and Catalysis Research Center, Hokkaido University, Sapporo 001-0021, Japan

Received: November 18, 2005; In Final Form: January 5, 2006

Surface-enhanced infrared absorption spectroscopy (SEIRAS) in the attenuated-total-reflection configuration (ATR-SEIRAS) has been applied for the first time to Ni electrodes. SEIRA-active Ni electrodes were obtained through initial chemical deposition of a 60-nm-thick Au underlayer on the reflecting plane of an ATR Si prism followed by potentiostatic electrodeposition of a 40-nm-thick Ni overlayer in a modified Watt's electrolyte. The Ni nanoparticle film thus obtained exhibited exceptionally enhanced IR absorption for the surface probe molecule CO while maintaining unipolar and normally directed bands. With the advantages of ATR-SEIRAS, free H<sub>2</sub>O molecules coadsorbed with CO at the Ni electrode were revealed, and their role in the electrooxidation of the CO adlayer at the Ni electrode is discussed. In addition, the conversion of bridge to linearly bonded CO at Ni electrode in a neutral solution was clearly identified upon electrooxidation of the CO adlayer. ATR-SEIRAS was also used to characterize the adsorption configuration of a pyridine adlayer at the Ni electrode. Both A<sub>1</sub> and B<sub>1</sub> modes of adsorbed pyridine were detected with comparably large intensities, essentially maintaining the spectral feature of pyridine molecules rather than that of "α-pyridyl species", which strongly suggests an "edge-tilted pyridine" configuration present at the Ni electrode, a configuration intermediate between the "end-on pyridine" and "edge-on α-pyridyl" adsorption modes reported in the literature.

### Introduction

Owing to its high signal sensitivity, simple surface selection rule, and negligible interference from bulk solution signals, surface-enhanced infrared absorption spectroscopy with the attenuated-total-reflection configuration (ATR-SEIRAS) is regarded as an important spectroscopic method for in situ characterization of surface adsorption and reaction, providing insight into the chemistry and physics of metal–electrolyte and metal–ambient interfaces.<sup>1–8</sup> So far, for in situ electrochemical applications, ATR-SEIRAS has been limited to coinage and platinum-group metal electrodes. Extension of this technique to other transition metal electrodes is highly desirable for it to become a general tool in surface electrochemistry. As an element of the iron group, nickel is a metal of both fundamental and practical interests in electrochemistry, surface science, and catalysis. To our best knowledge, ATR-SEIRAS at Ni electrodes has not been explored.

SEIRA originates from the interactions of IR photons with the metal atoms and adsorbed molecules; thin metal films consisting of nanoparticles particularly facilitate the SEIRA effect.<sup>2b,d,h</sup> The SEIRA activity depends greatly on the morphology of the metal nanoparticle film (simplified as nanofilm hereafter). Severely distorted bipolar or even inverted IR bands are often observed for transition metal nanofilms prepared by

evaporation or sputtering and electrodeposition.<sup>3,6a,9</sup> Appropriate fabrication of a conductive metallic nanofilm on an ATR IR window is essential for in situ ATR-SEIRAS. The most widely used ATR IR window is an undoped Si prism, which exhibits high stability in acidic and neutral electrolytes. The metallic films should be sufficiently conductive and have electrochemical features comparable to those of their bulk counterparts for use in electrochemistry. Moreover, they should be SEIRA-active without severely distorted or inverted bands to facilitate data analysis and explanation.

Very recently, SEIRA-active Pt-group metal nanofilms were obtained in our laboratory with a two-step wet process that incorporates an initial chemical deposition of a Au nanofilm on the basal plane of a Si prism with the subsequent electrodeposition of the desired Pt-group metal overlayers.<sup>8c,d</sup> This technique is somewhat similar to the sample preparation method used for surface-enhanced Raman spectroscopy (SERS) on transition metals. In the latter, the underlying Au layer functions as an amplifier of the Raman scattering of adsorbates on the transition metal, whereas it functions as a stable template for preparing SEIRA-active Pt-group metals in our case. The strategy circumvented several disadvantages associated with conventional dry processes (vacuum evaporation or sputtering), such as high-cost facilities, time-consuming procedures, poor enhancement reproducibility, bipolar band distortion, and sample contamination by organic species. We believe that this strategy can also be extended further to Ni electrodes for the following three reasons: First, theoretical calculations predict that nearly all metals can yield the SEIRA effect per se,<sup>2d,h</sup> without the need of borrowing the SEIRA effect from the underlying Au

\* Corresponding author. Phone: +86-21-55664050. Fax: +86-21-65641740. E-mail: wbc@fudan.edu.cn.

<sup>†</sup> Fudan University.

<sup>‡</sup> Shanghai University of Electric Power.

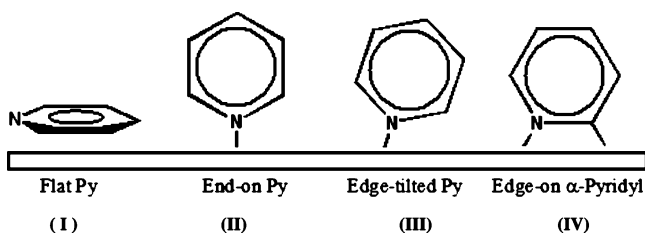
<sup>§</sup> Hokkaido University.

layer. Unlike SERS, in which a virtually pinhole-free metal layer with a thickness of a few atomic layers is required, the longer wavelengths of IR radiation allow for the deposition of a much thicker Ni overlayer carrying SEIRA activity. Second, electrodeposition of very thick Ni multilayers on Au from a modified Watt's solution is a quite mature technique, ensuring sufficiently "pinhole-free" Ni overlayers.<sup>10</sup> Third, Ni is easily passivated in neutral and alkaline electrolytes at high potentials without continuous active dissolution. This passivated layer can be electrochemically reduced back to nominal Ni. Thus, it can be expected that a very thick Ni overlayer (few tens of nanometers) on a Au underlayer should resemble bulk Ni in electrochemical behavior.

In the present work, CO was used as the probe molecule to examine the surface enhancement of Ni electrodes for the following reasons. External infrared reflection-absorption spectroscopy (IRAS) measurements of CO on Ni at solid-gas<sup>11–13</sup> and solid-electrolyte<sup>14a,15–17,18a,b</sup> interfaces have been reported. In particular, Cuesta and Gutiérrez systematically investigated pH effects on the CO adsorption sites and oxidation mechanism.<sup>15b</sup> As a result, these electrochemical and spectroscopic data can be used as references for the current study. Nevertheless, the reported CO bands in the literature are rather weak (around  $10^{-4}$ – $10^{-3}$  relative reflectance units,  $|\Delta R/R|$ ), and the signal-to-noise (S/N) ratio is poor, which, to some extent, prevented a detailed study of the dynamic oxidation process of CO at Ni electrodes such as the identification of coadsorbed water molecules.<sup>14a,15–17</sup> Recently, Wang et al.<sup>18a,b</sup> reported interesting abnormal IR effects (denoted as AIREs, i.e., inverted absorption and broadened bandwidth) in the external reflection configuration for Ni nanofilms electrodeposited on glassy carbon substrates via cycling potential control. The maximum absolute intensity of around  $8 \times 10^{-3}$  ( $\Delta R/R$ ) was obtained for their inverted major CO<sub>B</sub> band. However, the controversy over the origin of AIREs can complicate spectral analysis.<sup>2a,18c,19</sup> The normally directed CO<sub>B</sub> band was also detected under certain deposition conditions, but the band intensity was  $4 \times 10^{-4}$  ( $\Delta R/R$ ), only twice that of the polished bulk Ni electrode. By contrast, current ATR-SEIRAS studies on Ni electrodes yield normally directed and enhanced CO bands, with intensities as high as  $3.4 \times 10^{-2}$  ( $\Delta R/R$ ). The excellent S/N ratio for the surface signals of ATR-SEIRAS has two advantages: First, it enables simultaneous spectroscopic and electrochemical monitoring of the irreversible oxidation of CO adlayer at Ni electrode with a much better time resolution as compared to the previous linear potential scan (LPS) FT-IR method.<sup>15</sup> Second, new spectral features can be revealed such as bands for coadsorbed free water molecules at the Ni electrode, providing insight into the oxidation mechanism.

Significant enhancement of surface IR signals for the as-deposited Ni electrodes also allows for clarification of the adsorption configuration of pyridine (Py) at the Ni electrode. The orientations of Py at various metal surfaces in UHV and electrochemical environments have been extensively investigated by a variety of techniques, such as IRAS,<sup>20–22</sup> STM,<sup>8a,23</sup> HREELS,<sup>24</sup> ARUPS,<sup>24</sup> SERS,<sup>25,26</sup> SFG,<sup>27</sup> and isotope labeling,<sup>20,28</sup> in addition to electrochemical measurements.<sup>8a,20,22</sup> Three extreme modes of Py coordination to metal surfaces have been proposed (Chart 1): (1) "flat-lying Py" adsorption via  $\pi$  electrons of the aromatic ring (**I**, Chart 1), (2) N-coordinated vertical "end-on Py" adsorption (**II**, Chart 1), and (3) "edge-on  $\alpha$ -pyridyl" adsorption with nearly vertical orientation through the N and C(2) atoms (**IV**, Chart 1). In addition, intermediate configurations of the above critical modes have also been

**CHART 1. Related Adsorption Configurations for Py on Metal Surfaces<sup>a</sup>**



<sup>a</sup> (I) Flat-lying Py mode [e.g., Py at a Au(111) electrode at potentials sufficiently negative of the pzc<sup>8a,22</sup>], (II) end-on Py mode [e.g., Py at a Au(111) electrode at potentials positive of the pzc<sup>8a,22</sup>], (III) edge-tilted Py mode [e.g., Py at a Pt(111) surface in UHV at low temperature<sup>21</sup> and Py at a Ni nanofilm electrode (see text *vide infra*)], and (IV) edge-on  $\alpha$ -pyridyl mode [e.g., Py at Ni(100),<sup>24a</sup> Ni(111),<sup>24b</sup> Pt(111),<sup>21</sup> and W(011)<sup>29</sup> surfaces in UHV around room temperature].

reported,<sup>8a,21,26</sup> one of which is also shown as configuration **III** in Chart 1. The orientations and configurations depend on the electronic structure of the metal, the temperature, the coverage, the medium, and specifically the potential in the electrochemical system.<sup>8a,21,29</sup>

Although HREELS, XPS, and ARUPS measurements provided evidence of  $\alpha$ -pyridyl species formed on Ni surfaces in UHV at room temperature or higher,<sup>24,30</sup> SERS and density functional theory calculation results for Py adsorbed at a Ni electrode appeared to support the end-on adsorption geometry.<sup>31</sup> Because the SERS selection rule is rather complicated, however, the configuration of Py at a Ni electrode is still open for discussion according to our latest ATR-SEIRAS measurements.

## Experimental Section

**Ni Nanofilm Preparation and Characterization.** The prism used was an undoped Si hemicylinder (PASTEC, Osaka, Japan). The reflecting plane of the prism was polished with alumina slurries with decreasing particle sizes down to 0.05  $\mu\text{m}$ , followed by sonication in acetone and then water. Then, the Si hemicylinder was cleaned with the RCA method.<sup>8c</sup> Afterward, the reflecting surface was covered with 40% NH<sub>4</sub>F for 90 s to terminate the Si surface with hydrogen and was placed in the plating solution and 2% HF (2:1 by volume) for 3 min. Chemical deposition of Au was performed at 60 °C. The composition of the plating solution was 0.03 M AuCl<sub>3</sub>·HCl·H<sub>2</sub>O (adjusted to pH 8 with NaOH) + 0.3 M Na<sub>2</sub>SO<sub>3</sub> + 0.1 M Na<sub>2</sub>S<sub>2</sub>O<sub>3</sub>·5H<sub>2</sub>O + 0.1 M NH<sub>4</sub>Cl.<sup>2i,8c,d</sup> The Au-coated Si prism was rinsed with Milli-Q water (>18 M $\Omega$  cm) and assembled into a custom-made spectroelectrochemical cell by sandwiching an O-ring. Pt gauze and a saturated calomel electrode (SCE) were used as the counter and reference electrodes, respectively. The Au surface was then cleaned in 0.1 M HClO<sub>4</sub> by repeating potential scans between 0.0 and 1.45 V.

Deposition of a Ni overlayer on the as-deposited clean Au underlayer was conducted by electrolysis at  $-1.0$  V for 1800 s in a modified Watt's electrolyte (i.e.,  $10^{-3}$  M NiSO<sub>4</sub> +  $10^{-2}$  M H<sub>3</sub>BO<sub>3</sub> +  $10^{-4}$  M HCl).<sup>10</sup> Then, the spectroelectrochemical cell was thoroughly rinsed with copious amounts of Milli-Q water and immediately thereafter injected with 0.1 M K<sub>2</sub>HPO<sub>4</sub> + 0.1 M KH<sub>2</sub>PO<sub>4</sub> (phosphate buffer solution, pH 6.9). The potential was held at  $-1.20$  V for 10 min to reduce the native oxides on the Ni surfaces. The geometrical surface area of the Ni working electrode was 1.33 cm<sup>2</sup>. All electrolyte solutions were deaerated with high-purity Ar prior to measurements.

The double-layer capacitance of the Ni nanofilm electrode was obtained by measuring its differential capacitance curve in

a freshly prepared phosphate buffer solution by ac voltammetry in which a 100-Hz sinusoidal signal with an amplitude of 5 mV was superposed on a linear-scan dc potential at  $10 \text{ mV s}^{-1}$  from  $-1.0$  to  $0.2 \text{ V}$  and the ac current component was extracted and analyzed with a lock-in amplifier built in a CHI 660 B electrochemistry workstation (CH Instruments, Inc., Austin, TX).

The CHI 660B electrochemistry workstation was employed for all potential control in the electrodeposition of Ni nanofilms and subsequent (spectro)electrochemical measurements.

Inductively coupled plasma (ICP) atomic emission spectroscopy (AES) was used to determine the concentrations of dissolved Ni and Au ions from the metal films on Si in hot aqua regia of known volume. With known amounts of Au and Ni species, the thicknesses of the Au and Ni nanofilms were estimated to be around 60 and 40 nm, respectively, by assuming the same density as the bulk metals and using the geometric area for the calculations.

Atomic force microscopy (AFM) images of a Au nanofilm chemically deposited on Si before and after electrodeposition of a Ni overlayer were acquired in tapping mode under ambient conditions with a Pico-SPM (Molecular Imaging, Tempe, AZ). Si cantilevers having spring constants of between  $1.2$  and  $5.5 \text{ N m}^{-1}$  were used at resonance frequencies between 60 and 90 kHz.

XPS spectra of Ni-coated Au/Si samples were recorded on a Perkin-Elmer PHI-5000C ESCA system equipped with a dual X-ray source, using the Al K $\alpha$  radiation ( $h\nu = 1486.6 \text{ eV}$ ) anode and a hemispherical energy analyzer. The background pressure during data acquisition was maintained at  $10^{-9} \text{ Pa}$ . Measurements were performed at a pass energy of  $93.90 \text{ eV}$ . A survey XPS spectrum (0–1200 eV) and narrow spectra of all elements at high resolution were both recorded. Data were analyzed using the PHI-MATLAB software provided by PHI Corporation.

**In Situ ATR-SEIRA Spectroscopy.** The three-electrode system used for in situ ATR-SEIRAS is the same as that reported for the electrochemical measurements (vide supra). The detailed structure of the spectroelectrochemical cell and the ATR-SEIRAS measurements have been described elsewhere.<sup>1–8</sup> Briefly, unpolarized infrared radiation from a ceramic source was focused at the interface by being passed through the hemicylindrical Si prism at an incident angle of  $70^\circ$ , and the totally reflected radiation was detected. Spectra were acquired under either potentiostatic (multistep) or potentiodynamic (kinetics) mode. Infrared spectra were recorded on a Magna-IR ESP System 760 Fourier transform infrared spectrometer (Nicolet) equipped with a liquid-nitrogen-cooled MCT detector. The sample compartment of the FT-IR spectrometer was purged with  $20 \text{ L min}^{-1}$  of  $\text{CO}_2$ - and  $\text{H}_2\text{O}$ -free nitrogen. The spectrometer was operated at a resolution of  $4 \text{ cm}^{-1}$  (for multistep) or  $8 \text{ cm}^{-1}$  (for kinetics). Two hundred fifty-six interferograms were co-added to each single-beam spectrum in the multistep mode, whereas in kinetics mode, only four interferograms were collected for each spectrum. All spectra are shown in absorbance units defined as  $A = -\log(R/R_0)$ , where  $R$  and  $R_0$  represent the intensities of the infrared radiation reflected from the electrode at the sample and the reference potential, respectively. Reference spectra were measured at sufficiently positive potentials where CO was electrooxidized or most of the Py was desorbed from nominally reduced Ni surfaces.

## Results and Discussion

**AFM and XPS Characterization.** The morphology of a Ni-coated Au film prepared on a Si wafer plane by exactly the same preparation process as for the electrodes used in the

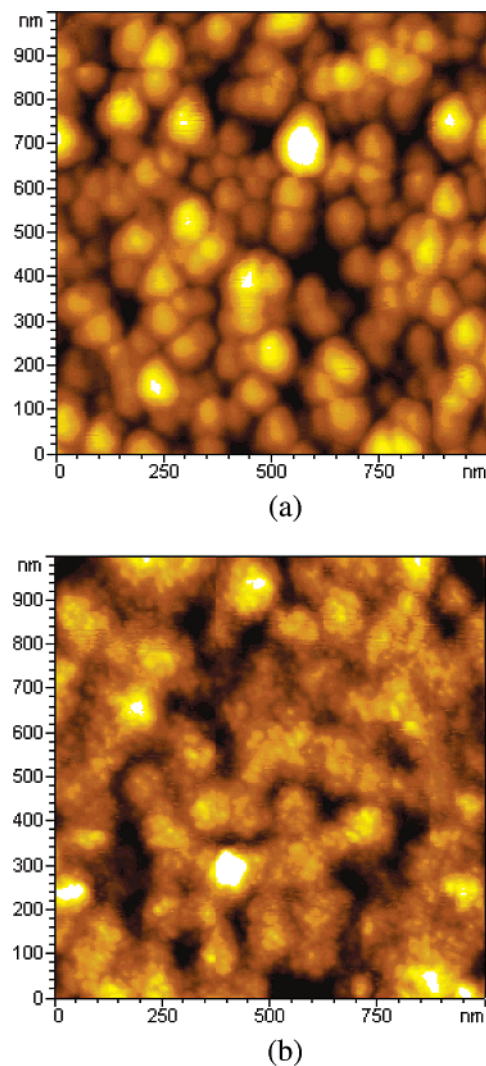


**Figure 1.** AFM images of (a) a Au underlayer (ca. 60 nm thick) chemically deposited on a Si wafer and (b) a Ni overlayer (ca. 40 nm thick) subsequently added by potentiostatic electrodeposition in a modified Watt's solution. Preparation conditions are detailed in the text.

spectroelectrochemical measurements was characterized with atomic force microscopy (AFM, Figure 1). For comparison, the AFM image of a bare Au underlayer is also shown. The thicknesses of the Au underlayer and Ni overlayer of the double-layer film were estimated to be about 60 and 40 nm, respectively, on average, based on the amount of each element contained in the film determined by ICP-AES after the film was dissolved in hot aqua regia. It can be seen that much finer Ni nanoparticles with a diameter of around 15 nm closely pack above the locus of the underlayer of larger Au nanoparticles. By contrast, the Ni nanofilm electrodeposited on a glassy carbon electrode by cycling potential deposition exhibited a layer structure.<sup>18a,b</sup> This difference in morphology between Ni nanofilms in the literature and those in the current work is probably of structural origin based on the requirements for producing AIREs and SEIRA effects.<sup>2d,3a,18a</sup>

The elemental composition of the surface layer of a Ni overlayer electrodeposited on a Au nanofilm chemically deposited on a Si substrate can be observed from a survey XPS spectrum, as shown in Figure 2. With the exception of the C (1s) peak, all of the other peaks could be assigned to photoemission and Auger transitions of Ni and O as indicated. The Ni ( $2p_{3/2}$ ) peaks at binding energies (BEs) of 852.4 and 854.5

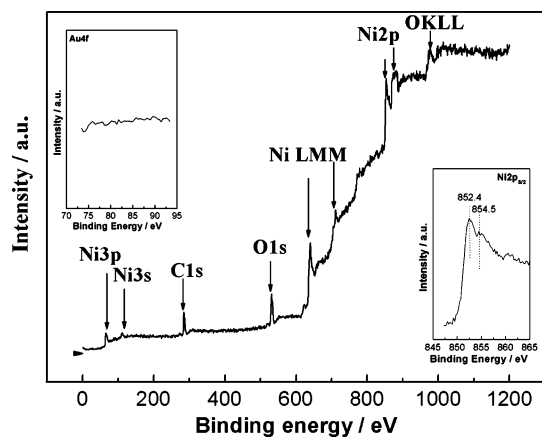


**Figure 2.** Survey XPS spectrum of an electrodeposited Ni overlayer (40 nm) on a Au nanofilm (60 nm) chemically deposited on a Si substrate and the narrow spectra of Au 4f and Ni 2p (insets).

eV in the right inset indicate that two types of Ni chemical species, one reduced and one oxidized, were detected. The peak at lower binding energy can be attributed to the metallic state, and that at higher energy indicates the presence of Ni species in the form of  $\text{Ni}^{2+}$  ions.<sup>32</sup> However, no Au peaks were observed, as shown in the left inset. Because XPS detects the elemental composition of surface layers with a skin depth of around 3–5 nm, the presence of Au–Ni alloys in the surface layers of our electrodeposited Ni nanofilm can be excluded, which ensures that all of the following (spectro)electrochemical results correspond to Ni electrodes.

**Electrochemical Characterization.** The as-deposited Ni nanofilm electrode was subjected to cathodic polarization at  $-1.20$  V for 10 min to remove the native nickel oxides. The cyclic voltammogram of the Ni electrode in a pH 6.9 phosphate buffer solution (solid trace in Figure 3a) shows an anodic peak at  $-0.34$  V with a charge of  $3.0 \text{ mC cm}^{-2}$  in the first forward potential scan. The anodic peak leads to the passivation of Ni at higher potentials. After a cyclic potential excursion, the electrode was set at  $-1.20$  V while CO was bubbled for 30 min to attain a saturated adsorption of CO. Subsequent cyclic voltammograms (dashed and dotted traces in Figure 3a) show that both hydrogen evolution and Ni electrooxidation were inhibited. In the presence of CO in solution, the anodic peaks were shifted positively to  $0.027$  V (dashed trace) and  $-0.017$  V (dotted trace). The charge in the first positive scan was  $5.9 \text{ mC cm}^{-2}$ , which was somewhat higher than that in the absence of CO, suggesting the mixed simultaneous electrooxidation of the Ni surface, chemisorbed CO, and dissolved CO.

Figure 3b shows the voltammetric responses in phosphate buffer solution following a saturated dosage of chemisorbed CO, obtained by bubbling in gaseous CO followed by Ar sparging. (Note that the same CO pre-dosing procedure for the Ni electrodes was used in the subsequent SEIRAS measurements.) The voltammogram in the first cycle (solid trace in Figure 3b) is similar to that in the CO-saturated solution (dashed trace in Figure 3a), which suggests that the adsorption of CO is strong. The voltammogram in the second cycle (dotted trace in Figure 3b) is also similar to that of the Ni electrode in Ar-saturated phosphate buffer solution (solid trace in Figure 3a), and the CO peak is no longer present, indicating that the chemisorbed CO had been electrooxidized in the first potential cycle.

All of the above voltammetric features are close to those reported for bulk polycrystalline Ni electrodes in the same electrolyte, which is essential for extending ATR-SEIRAS to the study of surface phenomena and processes at Ni electrodes.<sup>14b,c,15b</sup>

The surface roughness factor of the Ni nanofilm electrodes was estimated by taking the ratio of the measured double-layer capacitance to  $20 \mu\text{F cm}^{-2}$ , a commonly used reference value of the double-layer capacitance for a smooth metal electrode. Shown in Figure 4 presents a typical differential capacitance curve for a Ni nanofilm electrode as measured using ac voltammetry. The peak at  $-0.34$  V can be attributed to partial electrodisolution of the Ni surface, leading to surface passivation at potentials higher than  $-0.20$  V. At potentials negative of  $-0.70$  V, electrosorption and even the evolution of hydrogen can occur, contributing to the increased capacitance (i.e., pseudocapacitance). The practical double-layer region for a Ni electrode is rather narrow, roughly from  $-0.70$  to  $-0.40$  V as judged from Figure 4, which yields a double-layer capacitance of ca.  $87 \mu\text{F cm}^{-2}$ , corresponding to a surface roughness factor of ca. 4.3.

**SEIRAS of CO at Ni Electrodes.** Potential-dependent SEIRA spectra of a CO-pre-dosed Ni electrode obtained in multistep mode are shown in Figure 5. The bands at  $2000$ – $2050 \text{ cm}^{-1}$  can be assigned to linearly bonded CO ( $\text{CO}_L$ ), and those at  $1865$ – $1905 \text{ cm}^{-1}$  correspond to bridge-bonded CO ( $\text{CO}_B$ ).<sup>14a,15b</sup> It can also be seen that the  $\text{CO}_L$  bands are slightly sharper than the  $\text{CO}_B$  bands. The appearance of both  $\text{CO}_B$  and  $\text{CO}_L$  bands for a Ni electrode in a neutral electrolyte is in agreement with previous IRAS measurements.<sup>14a,15b</sup> A small band at  $2112 \text{ cm}^{-1}$  at relatively positive potentials can be attributed to CO chemisorbed on nickel oxide or on metallic Ni sites perturbed by the oxidation of the neighboring Ni atoms (this band is hereafter denoted as  $\text{CO}_{\text{Ni}^{\text{O}}}$ ).<sup>15a</sup> This band cannot be ascribed to linearly adsorbed CO on few (if any) exposed sites of the underlayer Au for the following reasons: First, the interaction of CO with Au is weak, and CO will nearly completely desorb when it is purged from solution.<sup>33</sup> Second, the linear CO band is located below  $2090 \text{ cm}^{-1}$  in neutral solution.<sup>34a</sup> Third, this band was not observed at lower potentials.

The potential-dependent spectra obtained by multistep FT-IR spectroscopy show that the Stark tuning rates are  $61.5$  and  $53.0 \text{ cm}^{-1} \text{ V}^{-1}$  for linear CO ( $\text{CO}_L$ ) and bridge CO ( $\text{CO}_B$ ), respectively. The former is in good agreement with the value measured for polycrystalline bulk Ni electrodes,<sup>15b</sup> and the latter is close to that obtained for Ni films electrodeposited on glassy carbon.<sup>18b</sup> Cuesta et al.<sup>15b</sup> detected a  $\text{CO}_B$  band with an intensity of  $8 \times 10^{-4} (\Delta R/R)$  for a bulk Ni electrode in pH 6.9 solution with IRAS. With AIREs, Wang et al.<sup>18b</sup> obtained a strong but abnormally inverted  $\text{CO}_B$  band with an intensity up to  $6 \times 10^{-3}$  for a Ni nanofilm electrodeposited on glassy carbon at pH 5.6. Using the formulation proposed by Griffiths et al.,<sup>3a</sup> they calculated the maximum surface enhancement factor to be 15.5. The  $\text{CO}_B$  band intensity herein observed is 0.015 absorbance unit or  $0.034 \Delta R/R$ , that is, 42.5 times stronger than that reported for bulk Ni electrodes and 5.7 times stronger than that for electrodeposited Ni films measured by AIREs. Precise calculation of the surface enhancement factor ( $G$ ) for the current Ni nanofilms is not easy. Nevertheless, if  $G$  is defined here as the ratio of band intensities between a molecule adsorbed on a Ni nanofilm and a molecule adsorbed on a smooth bulk Ni surface,<sup>2c</sup> after rational calibration of the surface coverage, surface roughness factor, incidence angle, and polarized state of IR radiation,  $G$  can be estimated to be larger than 29 (see Supporting Information). In addition, the CO bands obtained with ATR-SEIRAS are unipolar and normally directed in accordance with the definition of absorbance (i.e., normal absorption), facilitating the spectral analysis and interpretation. The asymmetry in CO bands with an extended “tail” toward

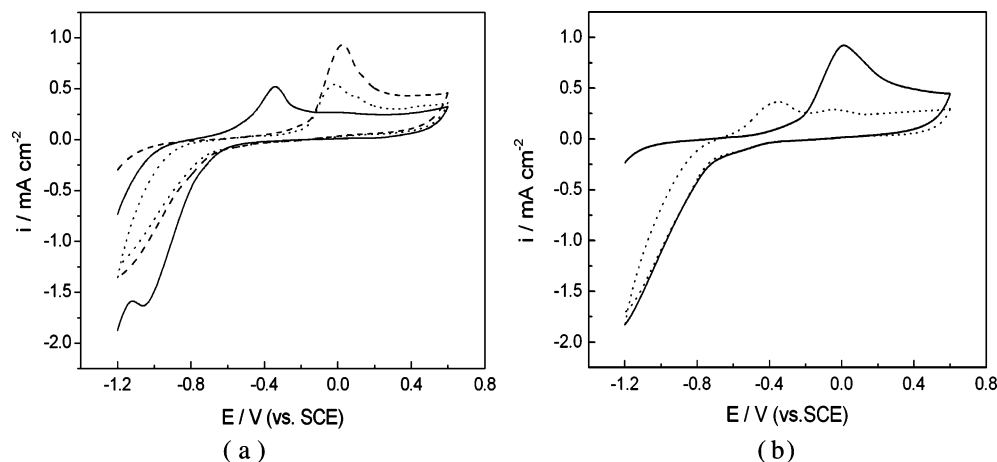


**Figure 3.** (a) Cyclic voltammograms of a Ni nanofilm electrode in 0.1 M phosphate buffer solution (pH 6.9) in high-purity Ar atmosphere (solid curve) and in CO-saturated solution (dashed and dotted curves for the first and second cycles, respectively). (b) Cyclic voltammograms of the CO-predosed Ni nanofilm electrode in a phosphate buffer solution after purging CO with Ar: first cycle (solid curve), second cycle (dotted curve). Scan rate = 50 mV s<sup>-1</sup>.

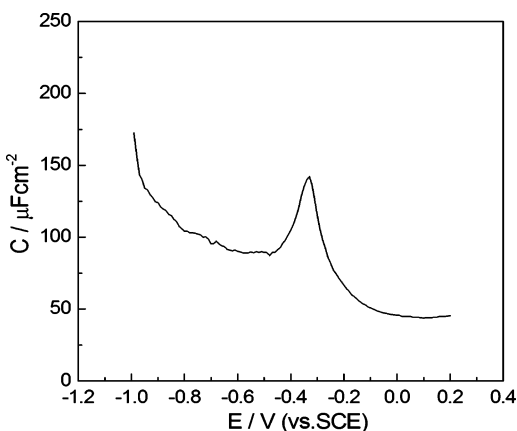


**Figure 4.** Differential capacitance curve for a Ni nanofilm electrode in 0.1 M phosphate buffer solution obtained with ac voltammetry. Experimental details can be found in the text.

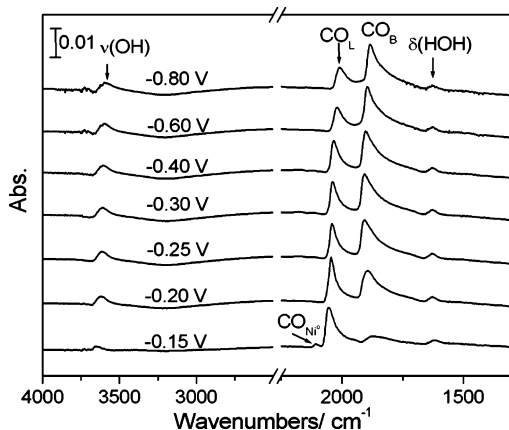


**Figure 5.** Potential-dependent multistep SEIRA spectra for a CO-predosed Ni nanofilm electrode in 0.1 M phosphate buffer solution. The reference potential is 0.60 V vs SCE, and the sample potentials are as indicated. The Ni electrode was predosed in CO-saturated 0.1 M phosphate buffer solution at -1.20 V SCE for 30 min, and then the dissolved CO was purged with Ar bubbling for 30 min.

lower wavenumbers can be partly ascribed to nanoparticle polydispersity.<sup>34b,34c</sup>

Previous IRAS measurements, including AIREs studies, of CO adsorption on Ni electrodes have not been able to detect coadsorbed free water bands because of their lower surface sensitivity and the interference of bulk water bands. By contrast,

free water molecules embedded in the CO adlayer on a Ni electrode surface (i.e., the hydrogen bonds between water molecules were broken) are readily identified in the current ATR-SEIRAS study. The sharp bands at 3592–3637 cm<sup>-1</sup> can be assigned to  $\nu(\text{OH})$ , and those at 1619–1626 cm<sup>-1</sup> can be assigned to  $\delta(\text{HOH})$  of free water molecules.<sup>2e,8c,35,36</sup> Specifically, the frequency of  $\nu(\text{OH})$  increases and that of  $\delta(\text{HOH})$  decreases with the potential. These water bands decrease in intensity with decreasing CO bands and become nearly invisible as the adsorbed CO adlayers are completely oxidized (vide infra). The decrease of coadsorbed free water bands has also been observed at Pt–Ru and Ru electrodes by Watanabe's group;<sup>6b</sup> at Pt electrodes by Okada's group;<sup>36</sup> and at Pd, Pt, Ru, and Rh electrodes by our group<sup>8c,8d</sup> using in situ ATR-SEIRAS.

Time-resolved measurements (kinetics mode) are more accurate for tracing an irreversible process, as compared to the above-mentioned multistep measurements. The ATR-SEIRA-active Ni nanofilms are highly beneficial for real-time monitoring and analysis of the electrooxidative removal of a CO adlayer at a Ni electrode. Figure 6 shows a series of 0.27-s-resolved spectra of a Ni-coated Au electrode predosed with CO in 0.1 M phosphate buffer solution, which were collected sequentially during a linear potential sweep (LPS) from -1.20 to 0.60 V at a scan rate 50 mV s<sup>-1</sup> (i.e., each successive spectrum was acquired for a period of 0.27 s over a potential interval of 13.5 mV.). The reference spectrum was taken at 0.60 V. The spectra at potentials positive of 0.05 V are not shown because of a large background undulation, which might be caused by passivation of the Ni surface. Figure 7 displays the plots of the normalized integrated intensities of the CO<sub>L</sub>, CO<sub>B</sub>, CO<sub>Ni</sub><sup>0</sup>,  $\nu(\text{OH})$ , and  $\delta(\text{HOH})$  bands against the potential and the corresponding voltammogram as well. The  $\nu(\text{OH})$  band of free H<sub>2</sub>O from -1.20 to -0.90 V in Figure 6 is not very distinct because it is buried in the relatively broad  $\nu(\text{OH})$  band of adjacent H<sub>2</sub>O layers, so its intensity in this region is not plotted. We tentatively attribute this result to the effect of hydrogen evolution at these negative potentials, which might change the hydrogen-bonding state of coadsorbed H<sub>2</sub>O molecules to some extent.<sup>36</sup>

The high surface sensitivity of ATR-SEIRAS provides insight into the adsorption and oxidation of CO adlayers at Ni electrodes. First, because the optical absorption coefficient of CO<sub>B</sub> is a factor of about 2.5 lower than that of CO<sub>L</sub>,<sup>15b</sup> the higher CO<sub>B</sub> band intensity indicates that CO<sub>B</sub> species are dominant at

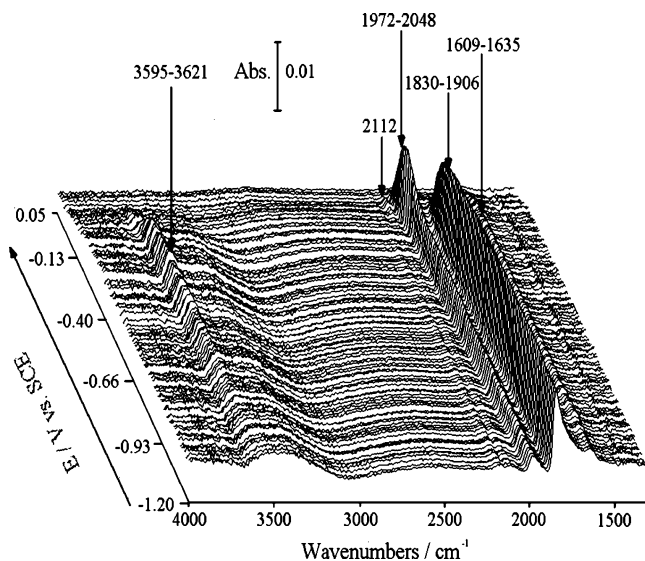


**Figure 6.** Series of time-resolved SEIRA spectra of a CO-predeposited Ni nanofilm electrode in 0.1 M phosphate buffer solution collected sequentially during a potential sweep cycling from  $-1.20$  to  $0.05$  V at  $50$   $\text{mV s}^{-1}$ . The time resolution used was  $0.27$  s. The Ni nanofilm electrode was predeposited in CO-saturated phosphate buffer solution at  $-1.20$  V for 30 min, and then the dissolved CO was purged with Ar bubbling for 30 min.

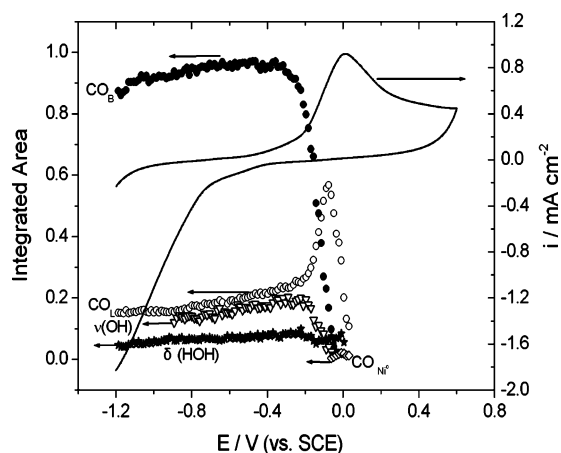


**Figure 7.** Cyclic voltammogram of a Ni-coated Au nanofilm electrode recorded at  $50$   $\text{mV s}^{-1}$  during in situ time-resolved ATR-SEIRA spectra measurements, along with the potential-dependent integrated intensities of the IR bands of  $\text{CO}_B$ ,  $\text{CO}_L$ ,  $\text{CO}_{\text{Ni}^0}$ , and coadsorbed water.

relatively low potentials. Second, it can be seen that, at potentials above  $-0.40$  V, the intensity of the  $\text{CO}_B$  band decreases monotonically and significantly as the oxidation of the CO adlayer proceeds, whereas that of the  $\text{CO}_L$  band first increases with decreasing  $\text{CO}_B$  and then starts to decrease as the concentration of  $\text{CO}_B$  becomes negligibly small. These trends strongly suggest that, in the oxidation process, the conversion of some  $\text{CO}_B$  to  $\text{CO}_L$  occurs with decreasing CO surface coverage. In other words,  $\text{CO}_L$  is more resistive than  $\text{CO}_B$  against electrooxidation at the Ni electrode. The transition of  $\text{CO}_B$  to  $\text{CO}_L$  at the Ni electrode with decreasing surface coverage is in accordance with the behavior measured for Ni(100) in UHV by FT-IRAS.<sup>13</sup> This feature is quite different from that found during oxidation of a CO adlayer at a Pd electrode, where  $\text{CO}_B$  is also dominant.<sup>8c</sup> In the latter,  $\text{CO}_L$  is first oxidized, and part of the  $\text{CO}_B$  is converted to CO adsorbed on hollow sites ( $\text{CO}_T$ ), but interconversion between  $\text{CO}_L$  and  $\text{CO}_B$  does not occur. Third, a new and rather weak band at  $2112$   $\text{cm}^{-1}$  attributable to  $\text{CO}_{\text{Ni}^0}$  appears at  $-0.07$  V and reaches a maximum at  $-0.03$

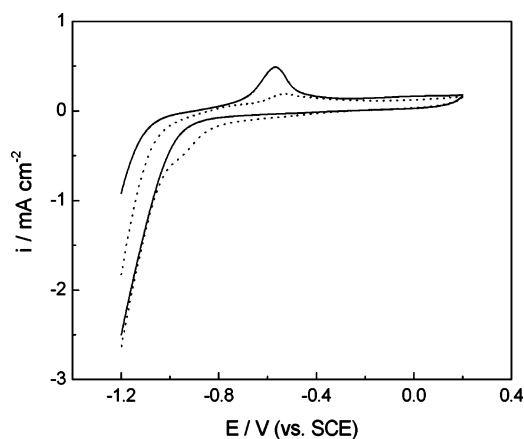


**Figure 8.** Cyclic voltammograms of a Ni nanofilm electrode in 0.1 M  $\text{KClO}_4$  solution in the absence (solid curve) and presence (dotted curve) of 10 mM Py recorded at  $50$   $\text{mV s}^{-1}$ .

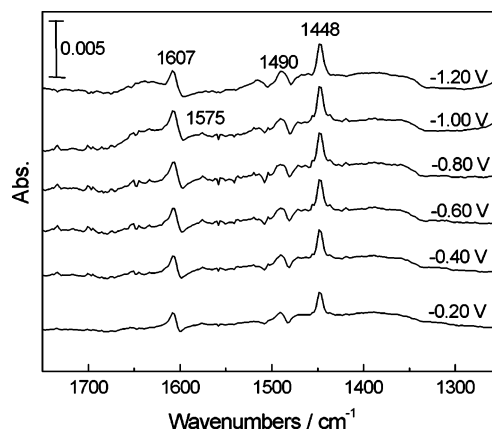


**Figure 9.** ATR-SEIRA spectra of adsorbed Py at the Ni-solution interface. The reference potential is  $0.20$  V vs SCE, and the sample potentials are as indicated. The solution contained 0.1 M  $\text{KClO}_4$  + 10 mM Py. Spectra are an average of 256 interferometer scans at each potential.

V, with nearly unchanged band position. It is also noted that the emergence of this  $2112$   $\text{cm}^{-1}$  band positively shifts by about  $0.10$  V as compared to that in the multistep measurements (see Figure 5), reflecting the advantage of time-resolved ATR-SEIRAS. Finally, it can be judged from Figures 5 and 6 that the  $\delta(\text{HOH})$  and  $\nu(\text{OH})$  bands for coadsorbed free  $\text{H}_2\text{O}$  decrease simultaneously in response to the sharp decrease of the  $\text{CO}_B$  band, suggesting that adsorbed CO molecules are oxidized by consuming the coadsorbed  $\text{H}_2\text{O}$  on the Ni electrode. In this regard, the active involvement of the coadsorbed  $\text{H}_2\text{O}$  in the oxidative removal of CO adlayers makes no difference for Ni- and Pt-group metal electrodes. In other words, activated free water molecules at these electrodes are likely oxygen donors for the electrooxidation of CO adlayers.<sup>34d,36</sup>

**SEIRAS of Pyridine (Py) at Ni Electrodes.** Significant enhancement of the surface IR signals for the as-deposited Ni electrodes also allows the examination of the adsorbed structure of Py at the Ni electrode. As mentioned in the Introduction, the formation of  $\alpha$ -pyridyl species on Ni surfaces upon Py adsorption has been well characterized in UHV systems by a variety of spectroscopic techniques. However, spectroscopic characterization of the configuration of Py adsorbed at Ni electrodes has been limited to only SERS. Tian's group succeeded for the first time in obtaining high-quality SER spectra of Py at a Ni electrode surface,<sup>25</sup> and they proposed an end-on configuration for the Py adlayer. One key piece of supporting evidence is the band at  $262$   $\text{cm}^{-1}$ , which was assigned to the metal-N vibration.

**TABLE 1. Wavenumbers and Assignments for Py at a Ni Electrode<sup>a</sup>**

liquid Py <sup>b</sup>	Py/Ni electrode <sup>c</sup>	Py/Au electrode, >pzc <sup>d</sup>	Py/Pt(111), UHV, low T <sup>e</sup>	$\alpha$ -pyridyl/Pt(111), UHV, room T <sup>e</sup>	assignments <sup>b</sup>	
					Wilson number	symmetry
1592 s	1607 s	1599 vs	1595 s	1568 vs	8a <sup>f</sup>	A <sub>1</sub>
1583 m	1575 vw	not detected	not detected	1568 vs	8b <sup>f</sup>	B <sub>1</sub>
1482 s	1490 m	1479 m	1470 m	1427 s	19a	A <sub>1</sub>
1439 vs	1448 vs	1448 w	1440 vs	1408 m	19b	B <sub>1</sub>

<sup>a</sup> Relative intensity: vs, very strong; s, strong; m, medium; w, weak; vw, very weak. <sup>b</sup> From ref 28. <sup>c</sup> Current result. <sup>d</sup> From ref 8a. <sup>e</sup> From ref 21. <sup>f</sup> When  $\alpha$ -pyridyl forms, it is difficult to assign the 1568 cm<sup>-1</sup> band exactly to 8a or to 8b; cf. refs 21 and 29.

The other piece of evidence is that the bands are predominantly assigned to the in-plane A<sub>1</sub> mode. Nevertheless, even though the 262 cm<sup>-1</sup> band can be ascribed to metal–N stretching, it does not necessarily indicate that the C<sub>2</sub> axis of Py is vertical with respect to the surface. In addition, the 262 cm<sup>-1</sup> band is also close to the calculated frequency (265 cm<sup>-1</sup>) for the  $\alpha$ -pyridyl–metal<sub>2</sub> symmetric stretching mode.<sup>26</sup> As a result, the 262 cm<sup>-1</sup> band in the SERS spectra cannot be exclusively assigned to the end-on configuration of adsorbed Py. On the other hand, the strict dipole selection rule based on counteraction of s-polarized light at metal surfaces in the “image-charge” theory, which applies to IR radiation (SEIRAS), does not exactly apply to SERS owing to the much lower electric conductivity of metals in the visible region.<sup>37–40</sup> Moreover, in SERS, one must consider the polarizability tensor  $\alpha$ , rather than the dipole moment  $\mu$ . Even simply based on an electromagnetic enhancement mechanism, A<sub>1</sub> modes have three Raman tensor components,  $\alpha_{xx}$ ,  $\alpha_{yy}$ , and  $\alpha_{zz}$ . In other words, the surface selection rule for SERS is not as straightforward as that for its counterpart SEIRAS. On the basis of the current ATR-SEIRAS measurements, we aim to clarify the adsorption geometry of Py at a Ni electrode.

Shown in Figure 8 are cyclic voltammograms for a Ni-coated Au electrode in 0.1 M KClO<sub>4</sub> without (solid trace) and with (dotted trace) 10<sup>-2</sup> M Py recorded at a scan rate of 50 mV s<sup>-1</sup>. It can be seen that the adsorption of Py significantly hinders the anodic dissolution and passivation of the Ni electrode but slightly promotes hydrogen evolution. Because of the high chemisorption energy for Py on Ni surfaces,<sup>24a</sup> even at rather negative potentials, Py does not desorb from the Ni surface, as will be revealed by SEIRA spectra. At the reference potential of 0.2 V, however, a fraction of Py molecules might still weakly adsorb at the nickel hydroxide surface.

Figure 9 shows the potential-dependent ATR-SEIRA spectra of Py adsorbed at a Ni electrode in 0.1 M KClO<sub>4</sub> and 0.01 M Py. Four bands at 1607, 1575, 1490, and 1448 cm<sup>-1</sup> correspond to  $\nu_{8a}(A_1)$ ,  $\nu_{8b}(B_1)$ ,  $\nu_{19a}(A_1)$ , and  $\nu_{19b}(B_1)$ , respectively, of adsorbed Py.<sup>28</sup> The relatively weak negative bands can be ascribed to Py adsorbed at the nickel hydroxide surface. Here, the A<sub>1</sub> and B<sub>1</sub> modes are in-plane vibrations yielding dipole changes along and perpendicular to the C<sub>2</sub> axis of Py, respectively. These bands and their assignments are listed in Table 1. For comparison, IR bands for liquid Py<sup>28</sup> and SEIRA bands for adsorbed Py at a Au(111) electrode<sup>8a</sup> are also tabulated. Both A<sub>1</sub> and B<sub>1</sub> modes appear for Py at a Ni electrode. In particular, the band at 1448 cm<sup>-1</sup>, a B<sub>1</sub> mode, is the most intense. According to the surface selection rule of SEIRAS, only those vibrations that cause dipole changes perpendicular to the metal surface are SEIRA-active.<sup>2b,d,h</sup> The simultaneous appearance of A<sub>1</sub> and B<sub>1</sub> modes suggests an edge-tilted Py adsorption geometry at the Ni electrode surface, with tilting of the C<sub>2</sub> axis edgewise apart from the normal to the Ni surface. The orientation and coordination of the adsorbed Py are nearly unchanged in the potential range from -1.20 to -0.20 V. In contrast, for Py adsorption on Au(111) electrodes at potentials

positive of the point of zero charge (pzc), the A<sub>1</sub> mode was predominant, and the B<sub>1</sub> mode was extremely weak, suggesting that a Py adlayer on the Au(111) electrode surface retains a mirror plane perpendicular to the molecular plane, i.e., the mirror plane containing the C<sub>2</sub> axis of Py and the surface normal are vertical with respect to the Py plane.

As mentioned before, HREELS, ARUPS, and XPS characterizations of Py adsorption at Ni(111) and Ni(100) in UHV indicate that exposures at elevated or room temperature produce an approximately vertically oriented species that can be attributed to the chemisorbed  $\alpha$ -pyridyl species. The question is whether the  $\alpha$ -pyridyl species is formed at Ni electrodes from the end-on configuration. To address this issue, a straightforward approach is to compare the spectral features of Py at a Ni electrode with those of  $\alpha$ -pyridyl species and edge-on Py species on metal surfaces. Fortunately, IRAS data for Py adsorption at Pt(111)<sup>21</sup> and W(110)<sup>29</sup> are available, which might lend some useful information for our judgment. For both edge-tilted Py and edge-on  $\alpha$ -pyridyl species, the original A<sub>1</sub> and B<sub>1</sub> modes are dipole-active. Yet, significant differences are found between the two surface species, as summarized in Table 1 (columns 4 and 5). First, the annealing of the substrate to room temperature results in the significant red shifts of the major bands associated with the conformation change from edge-tilted to  $\alpha$ -pyridyl species. Second, the conformation change also gives a significant change in relative intensities. The 19b mode (B<sub>1</sub>) at 1440 cm<sup>-1</sup> is the strongest for edge-tilted Py, whereas the 1568 cm<sup>-1</sup> band (which corresponds to the original 8a and/or 8b modes for pyridine) is the strongest for  $\alpha$ -pyridyl. Similar spectral features can be found for Py on the W(110) surface.<sup>29</sup> Our spectral pattern matches reasonably well with that of Py adsorption on Pt(111) at low temperature (see Table 1), suggesting that Py is adsorbed on the Ni electrode surface through the edge-tilted Py configuration without  $\alpha$ -C–H bond cleavage. This edge-tilted Py is likely a transitional configuration between the end-on Py and the edge-on  $\alpha$ -pyridyl species. For clarity, these three adsorption configurations can be found in Chart 1, in which the differentiation between plane-tilted and vertical orientations is not intended. Again, we demonstrate that the simple surface selection rule and high surface sensitivity of ATR-SEIRAS are very useful for characterization and analysis of molecular configurations at Ni electrodes, complementary to the widely used SERS technique.

## Conclusion

ATR-SEIRAS has been successfully extended for the first time to Ni electrodes. A two-step wet process was employed to fabricate SEIRA-active Ni electrodes, which incorporates an initial chemical deposition of a 60-nm-thick Au underlayer on the reflecting plane of an ATR Si prism and the subsequent potentiostatic electrodeposition of a 40-nm-thick Ni overlayer in a modified Watt's electrolyte. Significant enhancement was achieved without the emergence of bipolar or abnormally inverted absorption bands. The surface enhancement factor for

the Ni nanofilms thus obtained was evaluated to be more than 29 by comparing the band intensities of CO<sub>B</sub> species on a Ni nanofilm electrode and a mechanically polished Ni electrode with rational calibration. Real-time spectroscopic data indicate the active participation of coadsorbed free H<sub>2</sub>O molecules in the electrooxidation of a CO adlayer at a Ni electrode, as well as the conversion of bridge to linear CO. ATR-SEIRAS was also used to characterize the adsorption configuration of a Py adlayer at Ni electrodes. Both A<sub>1</sub> and B<sub>1</sub> modes of adsorbed Py were detected with appreciably large intensities, essentially maintaining the spectral features of Py molecules rather than those of  $\alpha$ -pyridyl species, suggesting an edge-tilted Py configuration present at the Ni electrode.

**Acknowledgment.** The NSFC (Nos. 20333040, 20473025), SRFDP (No. 20040246008), NCET (No. 04-0349), and SNPC (No. 0452NM064-2), China (W.B.C.), and the MEXT (No. 14205121 and Priority Areas 417), Japan (M.O.), are gratefully acknowledged for financial support. We also thank the State Key Laboratory for Physical Chemistry of Solid Surfaces, Xiamen University, Xiamen, China (No. 200303), for providing partial financial support and technical assistance.

**Supporting Information Available:** Evaluation of the surface enhancement factor (*G*). This material is available free of charge via the Internet at <http://pubs.acs.org>.

## References and Notes

- Hartstein, A.; Kirtley, J. R.; Tsang, J. C. *Phys. Rev. Lett.* **1980**, *45*, 201.
- (a) Nishikawa, Y.; Fujiwara, K.; Ataka, K.; Osawa, M. *Anal. Chem.* **1993**, *65*, 556. (b) Osawa, M. In *Handbook of Vibrational Spectroscopy*; Chalmers, J. M., Griffiths, P. R., Eds.; John Wiley & Sons: Chichester, U.K., 2002; Vol. 1, pp 785–799. (c) Miyake, H.; Osawa, M. *Chem. Lett.* **2004**, *33*, 278. (d) Osawa, M. *Bull. Chem. Soc. Jpn.* **1997**, *70*, 2861. (e) Ataka, K.; Yotsuyanagi, T.; Osawa, M. *J. Phys. Chem.* **1996**, *100*, 10664. (f) Ataka, K.; Nishina, G.; Cai, W. B.; Sun, S. G.; Osawa, M. *Electrochem. Commun.* **2000**, *2*, 417. (g) Miki, A.; Ye, S.; Senzaki, T.; Osawa, M. *J. Electroanal. Chem.* **2004**, *563*, 23. (h) Osawa, M.; Ataka, K.; Yoshii, K.; Niahikawa, Y. *Appl. Spectrosc.* **1993**, *47*, 1497. (i) Miyake, H.; Ye, S.; Osawa, M. *Electrochem. Commun.* **2002**, *4*, 973.
- (a) Bjerke, A. E.; Griffiths, P. R.; Theiss, W. *Anal. Chem.* **1999**, *71*, 1967. (b) Ishida, K. P.; Griffiths, P. R. *Anal. Chem.* **1994**, *66*, 522. (c) Bjerke, A. E.; Griffiths, P. R. *Appl. Spectrosc.* **2002**, *56*, 1275.
- Wandlowski, Th.; Ataka, K.; Pronkin, S.; Diesing, D. *Electrochim. Acta* **2004**, *49*, 1233.
- Shao, M. H.; Adzic, R. R. *J. Phys. Chem. B* **2005**, *109*, 16563.
- (a) Zhu, Y.; Uchida, H.; Watanabe, M. *Langmuir* **1999**, *15*, 8757. (b) Yajima, T.; Uchida, H.; Watanabe, M. *J. Phys. Chem. B* **2004**, *108*, 2654.
- Futamata, M.; Luo, L. Q.; Nishihara, C. *Surf. Sci.* **2005**, *590*, 196.
- (a) Cai, W. B.; Wan, L. J.; Noda, H.; Hibino, Y.; Ataka, K.; Osawa, M. *Langmuir* **1998**, *14*, 6992. (b) Cai, W. B.; Amano, T.; Osawa, M. *J. Electroanal. Chem.* **2001**, *500*, 147. (c) Yan, Y. G.; Li, Q. X.; Huo, S. J.; Ma, M.; Cai, W. B.; Osawa, M. *J. Phys. Chem. B* **2005**, *109*, 7900. (d) Yan, Y. G.; Li, Q. X.; Huo, S. J.; Sun, Y. N.; Cai, W. B. *Acta Chim. Sin.* **2005**, *63*, 545. (e) Huo, S. J.; Li, Q. X.; Yan, Y. G.; Chen, Y.; Cai, W. B.; Xu, Q. J.; Osawa, M. *J. Phys. Chem. B* **2005**, *109*, 15985.
- Lu, G. Q.; Sun, S. G.; Cai, L. R.; Chen, S. P.; Tian, Z. W. *Langmuir* **2000**, *16*, 778.
- (a) Lachenwitzer, A.; Magnussen, O. M. *J. Phys. Chem. B* **2000**, *104*, 7424. (b) Saraby-Reintjes, A.; Fleischmann, M. *Electrochim. Acta* **1984**, *29*, 557.
- Bailey, R. B.; Iri, T.; Richards, P. L. *Surf. Sci.* **1980**, *100*, 626.
- Surnev, L.; Xu, Z.; Yates, J. T. *Surf. Sci.* **1988**, *201*, 14.
- Grossmann, A.; Erley, W.; Ibach, H. *Surf. Sci.* **1996**, *355*, L331.
- (a) Hori, Y.; Koga, O.; Aramata, A.; Enyo, M. *Bull. Chem. Soc. Jpn.* **1992**, *65*, 3008. (b) Koga, O.; Hori, Y. *Electrochim. Acta* **1993**, *38*, 1391. (c) Hori, Y.; Murata, A. *Electrochim. Acta* **1990**, *35*, 1777.
- (a) Cuesta, A.; Gutiérrez, C. *J. Phys. Chem. B* **1997**, *101*, 9287. (b) Cuesta, A.; Gutiérrez, C. *Langmuir* **1998**, *14*, 3397.
- Zhao, M.; Wang, K.; Scherson, D. A. *J. Phys. Chem.* **1993**, *97*, 4488.
- (17) Ikemiya, N.; Suzuki, T.; Ito, M. *Surf. Sci.* **2000**, *466*, 119.
- (a) Wang, H. C.; Sun, S. G.; Yan, J. W.; Yang, H. Z.; Zhou, Z. Y. *J. Phys. Chem. B* **2005**, *109*, 4309. (b) Wang, H. C.; Zhou, Z. Y.; Tang, W.; Yan, J. W.; Sun, S. G. *Chin. Sci. Bull.* **2004**, *49*, 57. (c) Zheng, M. S.; Sun, S. G. *J. Electroanal. Chem.* **2001**, *500*, 223.
- Pecharomán, C.; Cuesta, A.; Gutiérrez, C. *J. Electroanal. Chem.* **2002**, *529*, 145.
- Ikezawa, Y.; Sawatari, T.; Kitazume, T.; Goto, H.; Toriba, K. *Electrochim. Acta* **1998**, *43*, 3297.
- (a) Haq, S.; King, D. A. *J. Phys. Chem.* **1996**, *100*, 16957.
- (a) Stolberg, L.; Morin, S.; Lipkowski, J.; Irish, D. E. *J. Electroanal. Chem.* **1991**, *307*, 241. (b) Lipkowski, J.; Stolberg, L. In *Adsorption of Molecules at Metal Electrodes*; Lipkowski, J., Ross, P. N., Eds.; VCH: New York, 1992; p 171. (c) Lipkowski, J.; Stolberg, L.; Morin, S.; Irish, D. E.; Zelenay, P.; Gamboa, M.; Wieckowski, A. *J. Electroanal. Chem.* **1993**, *355*, 147. (d) Hoon-Khoshla, M.; Fawcett, W. R.; Chen, A.; Lipkowski, J.; Pettinger, B. *Electrochim. Acta* **1994**, *39*, 1045. (e) Lipkowski, J.; Stolberg, L.; Yang, D.-F.; Pettinger, B.; Mirwald, S.; Henglein, F.; Kolb, D. M. *Electrochim. Acta* **1994**, *39*, 1045. (f) Li, N.; Zamylny, V.; Lipkowski, J.; Henglein, F. *J. Electroanal. Chem.* **2002**, *524–525*, 43.
- (a) Wan, L. J.; Wang, C.; Bai, C.; Osawa, M. *J. Phys. Chem. B* **2001**, *105*, 8399. (b) Wang, D.; Xu, Q. M.; Wan, L. J.; Wang, C.; Bai, C. L. *Langmuir* **2002**, *18*, 5133.
- (a) Dinardo, N. J.; Avouris, Ph.; Demuth, J. E. *J. Chem. Phys.* **1984**, *81*, 2169. (b) Cohen, M. R.; Merrill, R. P. *Langmuir* **1990**, *6*, 1282.
- (a) Ren, B.; Tian, Z. Q.; Wu, D. Y. *J. Phys. Chem. B* **2004**, *108*, 9463. (b) Huang, Q. J.; Lin, X. F.; Yang, Z. L.; Hu, J. W.; Tian, Z. Q. *J. Electroanal. Chem.* **2004**, *563*, 121. (c) Ren, B.; Huang, Q. J.; Cai, W. B.; Mao, B. W.; Liu, F. M.; Tian, Z. Q. *J. Electroanal. Chem.* **1996**, *415*, 175.
- Zuo, C.; Jagodzinski, P. W. *J. Phys. Chem. B* **2005**, *109*, 1788.
- Tadjeddine, A.; Le Rille, A.; Pluchery, O.; Vidal, F.; Zheng, W. Q.; Peremans, A. *Phys. Status Solidi A* **1999**, *175*, 89.
- Corsin, L.; Fax, B. J.; Lord, R. C. *J. Chem. Phys.* **1953**, *21*, 1170.
- Andersson, M. P.; Uvdal, P. *J. Phys. Chem. B* **2001**, *105*, 9458.
- Bridge, M. E.; Connolly, M.; Lloyd, D. R.; Somers, J.; Jakob, P.; Menzel, D. *Spectrochim. Acta* **1987**, *43A*, 1473.
- Wu, D. Y.; Duan, S.; Ren, B.; Tian, Z. Q. *J. Raman Spectrosc.* **2005**, *36*, 533.
- Casella, I. G.; Guascito, M. R.; Sannazzaro, M. G. *J. Electroanal. Chem.* **1999**, *462*, 202.
- Sun, S. G.; Cai, W. B.; Wan, L. J.; Osawa, M. *J. Phys. Chem. B* **1999**, *103*, 2460.
- (a) Tadայyoni, M. A.; Weaver, M. J. *Langmuir* **1986**, *2*, 179. (b) Park, S.; Wieckowski, A.; Weaver, M. J. *J. Am. Chem. Soc.* **2003**, *125*, 2282. (c) Park, S.; Wieckowski, A.; Weaver, M. J. *J. Phys. Chem. B* **2001**, *105*, 9719. (d) Kim, H.; Rabelo de Moraes, I.; Tremiliosi-Filho, G.; Haasch, R.; Wieckowski, A. *Surf. Sci.* **2001**, *474*, L203.
- (a) Yoshimi, K.; Song, M. B.; Ito, M. *Surf. Sci.* **1996**, *368*, 389. (b) Ito, M.; Nakamura, M. *Faraday Discuss.* **2002**, *121*, 71.
- Shiroishi, H.; Ayato, Y.; Kunimatsu, K.; Okada, T. *J. Electroanal. Chem.* **2005**, *581*, 132.
- Brolo, A. G.; Irish, D. E. *J. Electroanal. Chem.* **1996**, *414*, 183.
- Moskovits, M.; DiLella, D. P.; Maynard, K. J. *Langmuir* **1988**, *4*, 61.
- Creighton, J. A. *Surf. Sci.* **1983**, *124*, 209.
- (a) Pettinger, B. In *Adsorption of Molecules at Metal Electrodes*; Lipkowski, J., Ross, P. N., Eds.; VCH: New York, 1992; pp 285–345.